

**Factors Affecting the Nucleus-Independent Chemical  
Shift in NMR Studies of Microporous Carbon Electrode  
Materials**

## Abstract

NMR spectroscopy has recently emerged as a powerful method for studying electrolyte species in microporous carbon electrodes used in capacitive energy storage devices. Key to this approach is the nucleus-independent chemical shift (NICS) which enables adsorbed species to be distinguished from those in the bulk electrolyte. The magnitude of the NICS is well known to be dependent on the distance of the adsorbed species from the carbon surface, and has therefore been used in several studies as a probe of the carbon pore size. However, the NICS can also be influenced by a number of other structural and chemical factors which are not always taken into account. To investigate this, we have carried out a systematic study of the factors influencing the NICS of aqueous electrolyte species adsorbed on polymer-derived activated carbon [in the absence of an applied potential](#). We find that a number of effects arising from both the carbon structure as well as the behaviour and chemical properties of the electrolyte species can contribute to the observed NICS ~~and must be taken into account when interpreting NMR spectra of microporous carbon electrode materials~~. In turn, the measurement of these effects provides important information about ion behaviour and reveals significant differences in the adsorption behaviour of different ions in the absence of an applied potential. In accordance with several computational studies, we find experimental evidence that the local concentration of spontaneously adsorbed alkali ions decreases with the pore size. This has potential implications for understanding the molecular-level mechanism of charge storage in capacitive devices.

## Introduction

Supercapacitors are high-power energy storage devices which function through the electrosorption of ions on microporous carbon electrodes. Most commercial supercapacitor devices employ organic electrolytes due to their moderate voltage window and good ionic conductivity.[1] However, there has been considerable recent interest in the development and study of aqueous electrolytes based on inorganic salts.[2-5] Aqueous electrolytes have the combined advantages of being relatively cheap, environmentally-friendly and simple to prepare and handle.[6] Furthermore, they are also relevant to the closely related technology of capacitive ~~deionization~~ salination (CDI) which employs the same capacitive mechanism for the energy-efficient production of fresh water.[7, 8] However, despite the growing interest in both supercapacitor and CDI devices, the precise details of the properties and behaviour of aqueous electrolyte ions within microporous electrodes is still not well understood and continues to be the subject of extensive research. Most of the progress in this area has come from theoretical modelling which has led the way in building up a microscopic picture of the behaviour of aqueous ions in confined environments. Over the last decade numerous studies have revealed that factors such as specific ion properties,[9] relative pore/ion sizes,[10-12] and ion solvation energies[13, 14] can have a strong influence on adsorption phenomena, with important implications for the charging mechanisms in electrochemical devices. One important factor recently discussed in the literature is the relative “ionophobicity” of the system, or the propensity of the ions to enter the pores before charging, has been shown to have significant effects on the charging dynamics and energy capacity.[15, 16]. Therefore to fully understand the factors influencing the charging mechanism, it is also necessary to have a detailed picture of the ion-pore system in the absence of an applied potential.

While progress has been made by theoretical modelling, experimental insight has been limited owing to the structural complexity of microporous carbons and the dynamic nature of the adsorbed species.

One of the few techniques that has provided insight is the electrochemical quartz crystal microbalance method which has made significant progress in monitoring ion uptake during charging of microporous electrodes and has enabled different charging regimes to be identified.[17-20] This technique has also been extended to simultaneously monitor mechanical changes in electrode properties.[21-24] Small-angle neutron scattering has also been used to selectively measure ion concentrations in micropores of different sizes under different states of charge.[25, 26] Another technique that has recently gained prominence for studying ion adsorption in porous carbons is NMR spectroscopy. NMR has the advantage that it is element selective and so can be used to observe a specific species in isolation, and is also fully quantitative such that adsorbed ions and solvent species can be independently 'counted' in the uncharged or charged state.[27, 28] The key phenomenon that allows this is the so-called nucleus-independent chemical shift (NICS), which arises from the magnetic shielding due to circulation of electrons in the carbon surface, thereby enabling adsorbed species to be distinguished from those in bulk solution.[29-33] The magnitude of the NICS is dependent on the distance of the adsorbed species from the carbon surface and has therefore been used as a probe of the carbon pore size.[34-36] However, recent studies have started to reveal that additional factors such as the carbon domain size and exchange phenomena also contribute to the observed NICS, meaning that these need to be accounted for when interpreting experimental data.[37-39]

One of the other challenges in studying adsorption phenomena in microporous carbons is the complexity and diversity of carbon structures. Microporous carbons can be produced by several different methods from many organic and inorganic precursors, leading to a wide range of pore diameters, pore size distributions, interpore connectivities and dopants or functional groups. While a high degree of local graphene-like ordering can be present, characterisation of longer range structural properties is very challenging owing to the high degree of disorder. For the study of adsorption phenomena, it is desirable to use a model system where one or more of these parameters can be varied

systematically. An example of such a system is microporous carbons derived from pyrolysis and activation of polyether ether ketone (PEEK) polymer. PEEK-derived carbons (PDCs) have a simple synthesis procedure which produces a high-surface area microporous carbon where the pore structure can be easily influenced through the activation conditions.[40-42] For this reason, PDCs have been used as a model system in a number of NMR studies of microporous carbon adsorption phenomena.[34, 35, 43-46] In particular, Xing *et al.* used density functional theory calculations to relate the magnitude of the observed NICS to the pore size, and on this basis proposed a simple NMR methodology for characterising the pore size distribution in PDCs.[35] This approach has been extended to gain insight into pore filling phenomena in similar materials.[43, 46] However, such “NMR porosimetry” approaches rely on the assumption that the magnitude of the NICS is primarily influenced by the proximity of the adsorbed species to the carbon surface. While this may be valid when comparing the same species in different PDCs, it may be necessary to account for additional contributions to the NICS when comparing different species in the same system (*e.g.*, ions and solvent molecules).

To investigate the factors that contribute to the NICS, in this work we have carried out a systematic NMR study of the adsorption of aqueous alkali metal chloride solutions [in the absence of an applied potential](#) using PDCs as a model system. Our investigation shows that the NICS can vary significantly owing to a range of effects related to both the carbon structure and differences in the chemical properties of the adsorbed species. We first show that the standard PDC synthesis procedure produces [highly-inhomogeneously activated](#) samples with a large pore size distribution which is not ideal for systematic adsorption investigations. Through optimisation and careful control of the synthesis conditions, it is possible to produce [thoroughly activated carbon particles](#)~~more homogeneous samples~~ within which a [reproducible](#) multimodal micropore size distribution is ~~identified~~[obtained](#). This allows the observation of significant differences in NICSs for a range of aqueous alkali metal cations adsorbed within PDCs with the same or similar pore size distributions. We show that by taking into

account the range of micropore environments that are present, together with the different chemical properties of the aqueous alkali metal cations, the differences in the NICS of the adsorbed species can then be rationalised. We also observe an additional concentration dependence of the NICS which suggests that, in the absence of an applied potential, larger pores are preferentially occupied by ions when low electrolyte concentrations are used. This is consistent with a number of theoretical studies which predict significant pore-size dependent energy barriers for the entry of hydrated ions to micropores. These observations highlight important factors that should be taken into account when using NMR as a probe of microporous carbon structure and are also discussed in terms of their implications for the charging mechanism in electrochemical devices.

## Experimental and Computational Details

PDCs were synthesised following a procedure similar to others in the literature.[35, 42] PEEK polymer was first carbonised in an alumina boat within a tube furnace at 900°C under flowing N<sub>2</sub> gas before being cooled to room temperature. The resulting carbon slug was ground into particles of approximately 0.5 mm diameter before being subjected to a steam activation step where the sample was heated in an alumina boat at 900°C under flowing N<sub>2</sub> gas that was bubbled through deionised H<sub>2</sub>O in a Dreschel bottle before entering the tube furnace. During steam activation, the main mechanism of the development of pore volume is the reaction of carbon with H<sub>2</sub>O to form gaseous products which leave the structure.[47] The extent of steam activation can therefore be parameterised by the mass loss, or burn-off (BO) value, which is defined as the percentage mass difference of the carbonised sample before and after steam activation.[42, 48] In this work steam activation durations of between 145 – 75 minutes resulted in BO values of between 21~~36~~ – 62 %.

Solid-state NMR experiments were performed using a 400 MHz Bruker Avance III HD WB spectrometer operating at a magnetic field strength of 9.4 T. Samples were loaded into 3.2 mm outer-

diameter zirconia rotors and the solutions were injected with a microsyringe, after which a PTFE plug was inserted to avoid evaporation or leaking. [Apart from the build up experiments, all PDC samples were soaked with a volume of H<sub>2</sub>O or salt solution that was at least 1.5 times the pore volume \(as measured by gas sorption\) to ensure that the system was fully saturated.](#) The magic-angle spinning (MAS) rate was 5 kHz. For each sample the recycle interval was set to at least 5 x T<sub>1</sub> (as measured by a saturation recovery experiment) and the 90° pulse length was optimized for each sample to ensure that spectra were recorded under quantitative conditions. <sup>1</sup>H spectra were recorded using the DEPTH pulse sequence,[49] with 16 scans, recycle intervals between 3 – 5 s and 90° pulses between 2 – 3 μs. The spectra of cations were recorded using a single pulse sequence, with a number of scans depending on the concentration, ranging from 32 (1 mol L<sup>-1</sup>) to 10,000 (0.05 mol L<sup>-1</sup>), and 90° pulse lengths between 2 - 6 μs. Recycle intervals were 0.2 s, 0.01 s and 3 s for <sup>23</sup>Na, <sup>87</sup>Rb and <sup>133</sup>Cs respectively, and ranged from 2 – 6 s for <sup>7</sup>Li. Two-dimensional exchange experiments were acquired with 16 scans for each of the 800 t<sub>1</sub> increments. In the indirect dimension the spectral width was set to 8 kHz to minimise the number of t<sub>1</sub> increments required and the States-TPPI protocol[50] was used to achieve sign discrimination. The recycle interval was 0.2 s and the 90° pulse length was 1.8 μs. <sup>1</sup>H spectra were referenced relative to deionised H<sub>2</sub>O (4.8 ppm) and <sup>7</sup>Li, <sup>23</sup>Na, <sup>87</sup>Rb and <sup>133</sup>Cs spectra were referenced relative to neat 1M aqueous solutions of the corresponding metal chloride (0 ppm in each case).

All solid-state NMR spectra were deconvoluted using the DMfit program[51] to yield resonance intensity and width with a Gaussian-to-Lorentzian ratio between 0 and 1, as well as estimated errors, which depended on the resonance intensity. For <sup>1</sup>H, the ex-pore resonance was fitted with one component, and the in-pore resonance with two components, while two spinning sidebands were fitted with a single component. The fitting errors were below 2% (intensity) and below 10% (width). For the ions, no spinning sidebands were observed, and both ex-pore and in-pore resonances required

only one component. The fitting errors were larger for dilute solutions, but overall were below 5% (intensity) and 10% (width).

Solution state NMR diffusion measurements were acquired on a 400 MHz Bruker Avance III spectrometer, operating at a field strength of 9.4 T. The temperature was calibrated at 298.0 K using MeOH-d<sub>4</sub>.<sup>[52]</sup> The pulsed field gradients were calibrated using the standard 1% H<sub>2</sub>O/D<sub>2</sub>O solution doped with 0.1 mg/ml GdCl<sub>3</sub> with a known diffusion coefficient of  $1.90 \times 10^{-9}$  m<sup>2</sup>/s, giving a nominal maximum gradient strength of 55.8 G/cm. All diffusion data were acquired with a single stimulated echo sequence using bipolar diffusion-encoding gradients<sup>[53]</sup> with a spoil gradient applied at the beginning of the diffusion period (stebppg1s). Datasets were acquired with 8 transients and 16 gradient strength increments in linear steps from 10% to 95% of the full strength, using rectangular gradients with half-sine ramped shapes at the beginning and end (SMSQ10.100). For <sup>1</sup>H<sub>2</sub>O measurements the repetition time was  $5 \times T_1$ , while for <sup>7</sup>Li, <sup>23</sup>Na and <sup>133</sup>Cs it was  $1.3 \times T_1$ . This shorter than usual recycle delay was empirically verified to not alter the measured D. The diffusion parameters were as follows: H<sub>2</sub>O:  $\Delta$  40 ms,  $\delta$  1.4 ms, 95% attenuation; <sup>7</sup>Li:  $\Delta$  250 ms,  $\delta$  3 ms, 95%; <sup>23</sup>Na:  $\Delta$  50 ms,  $\delta$  4 ms, 70%; <sup>133</sup>Cs:  $\Delta$  250 ms,  $\delta$  3 ms, 95%. Peak areas<sup>[54]</sup> were fitted to the appropriate Stejskal-Tanner equation using Dynamics Center within Bruker Topspin software to determine the diffusion coefficient.

Nitrogen gas sorption measurements were carried out at 77 K using a Quantachrome Autosorb instrument. Prior to each experiment, the samples were outgassed at 300 °C for 28 hours at  $10^{-5}$  Pa. Data was treated in ASiQwin using the QSDFT method on the adsorption branch assuming slit/cylindrical pores.

Dynamic Light Scattering (DLS) analyses were carried out using a Malvern Mastersizer 3000 assuming the refractive index of graphite, *i.e.*, 2.68. Samples were suspended in water until an obscuration of 1-10% was achieved, and particle size distributions were then extracted using the built-in “general purpose” method.

Born-Oppenheimer molecular dynamics simulations were performed using the QUICKSTEP module of CP2K version 3.0 on cells with periodic boundary conditions containing a single cation and 64 water molecules.[55, 56] Temperature and pressure were kept constant using a NPT\_I ensemble, where the simulation cell is isotropic with a 0.5 fs time step. Initial cubic cell parameters were set to  $a = b = c = 11.99 \text{ \AA}$ , an average temperature  $T=400 \text{ K}$  (to ensure a liquid water environment when using the exchange correlation functional specified below) was maintained using a Nosè-Hoover thermostat and a barostat maintained pressure of 1 atm.[57] The Gaussian Augmented Plane Wave method (GAPW) was used for the calculation of forces and energies, which uses a Gaussian basis set with augmented plane wave pseudopotentials.[58] The Perdew-Burke-Ernzerhof (PBE) generalised gradient approximation[59] was used to calculate the exchange correlation energy including the DFT-D3 dispersion correction as proposed by Grimme.[60] The calculations used a double- $\zeta$  polarization quality Gaussian basis sets (DZVP-MOLOPT-SR-GTH) and a planewave cutoff of 500 Ry.[61] Charge neutrality was achieved through the use of a uniform neutralising background charge. Each calculated trajectory was 20 ps long and was comprised of 40,000 steps, each of length 0.5 fs. The first 5 ps of each trajectory was treated as an equilibration period, in keeping with previous studies,[62-68] and was not considered in consequent analysis.

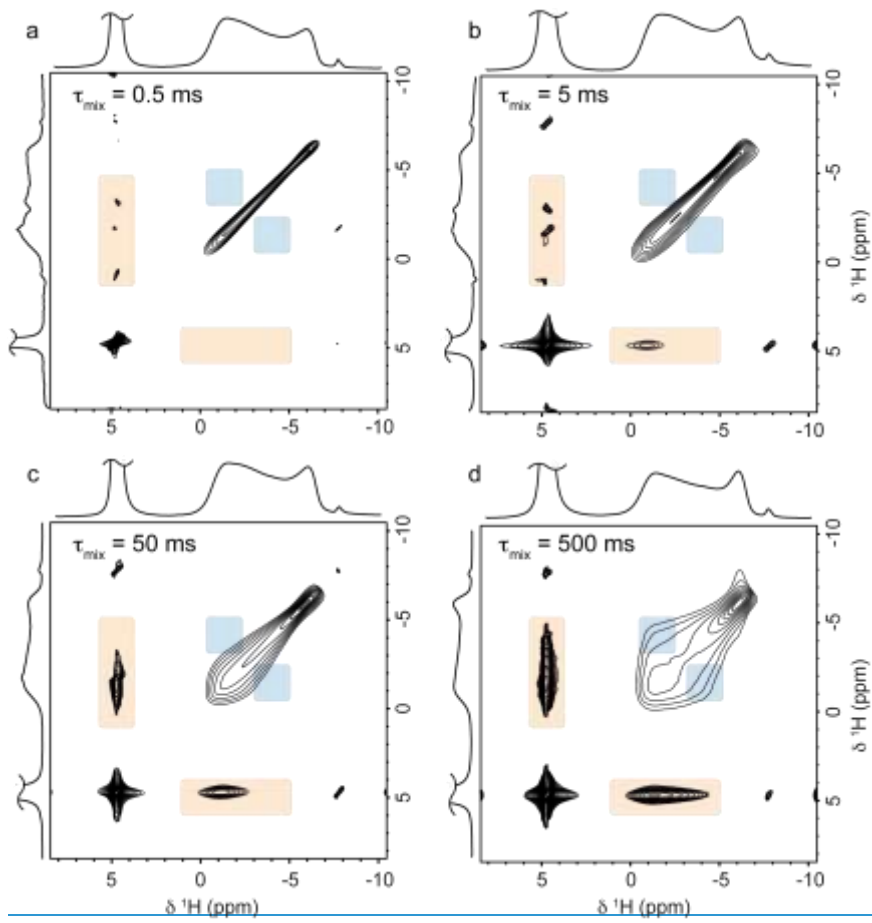
## Results

**Effect of Sample Homogeneity and Pore Structure.** Figure 1 shows  $^1\text{H}$  MAS NMR spectra of PDC samples with burn-offs between 0 – 55% which were saturated with deionised  $\text{H}_2\text{O}$ . In each spectrum,

the sharp ex-pore resonance at  $\delta = 4.8$  ppm corresponds to bulk water between the carbon particles, while in-pore resonances due to adsorbed H<sub>2</sub>O molecules are shifted by the NICS to between  $\delta = -1$  and  $-6$  ppm. For the BO = 0% sample (*i.e.*, carbonised PEEK that was not subjected to steam activation), the observation of an in-pore resonance shows that the carbonisation process itself results in some degree of intrinsic porosity which is accessible to H<sub>2</sub>O molecules. The large NICS of 10.8 ppm suggests that these intrinsic pores are very small – approximately 0.8 nm in width based on DFT calculations of a circumcoronene slit pore.[36] The spectra of PDCs with BO = 36 – 55% exhibit in-pore resonances with smaller NICSs, which is expected due to the larger pores that steam activation introduces into the carbon structure. However, in all three steam-activated PDCs, the in-pore lineshape is broad and asymmetric, with significant intensity remaining at  $\delta = -6$  ppm. To investigate the origin of these features, two-dimensional exchange spectra were recorded on the BO

**Figure 1:**  $^1\text{H}$  MAS NMR spectra of PDCs with burn-offs between 0 – 55%, saturated with deionised  $\text{H}_2\text{O}$ . The red area from -4 ppm to -7 ppm highlights the region of the in-pore feature corresponding to  $\text{H}_2\text{O}$  molecules in intrinsic micropores resulting from the carbonisation process. Asterisks denote spinning sidebands.

and -6 ppm. For the BO = 0% sample (i.e., carbonised PEEK that was not subjected to steam activation), the observation of an in-pore resonance shows that the carbonisation process itself results in some degree of intrinsic porosity which is accessible to  $\text{H}_2\text{O}$  molecules. The large NICS of 10.8 ppm suggests that these intrinsic pores are very small - approximately 0.8 nm in width based on DFT calculations of a circumcoronene slit pore.[36] The spectra of PDCs with BO = 36 - 55% exhibit in-pore resonances with smaller NICSs, which is expected due to the larger pores that the steam activation introduces into the carbon structure. However, in all three steam-activated PDCs, the in-pore lineshape is broad and asymmetric, with significant intensity remaining at  $\delta = -6$  ppm. To investigate the origin of these features, two-dimensional exchange spectra were recorded on the BO = 45% sample (Figure 2). For the shortest mixing time,  $\tau_{\text{mix}}$ , of 0.5 ms (Figure 2a), the in-pore resonance is confined to the diagonal line, showing that the broadening of this resonance is inhomogeneous, meaning that i.e., the water molecules occupy a range of pore environments leading to a distribution of NICS values. For a longer mixing time of 5 ms (Figure 2b), off-diagonal correlations between ex-pore resonance and the in-pore resonance with smallest NICS signify exchange on this timescale between species adsorbed in the largest pores



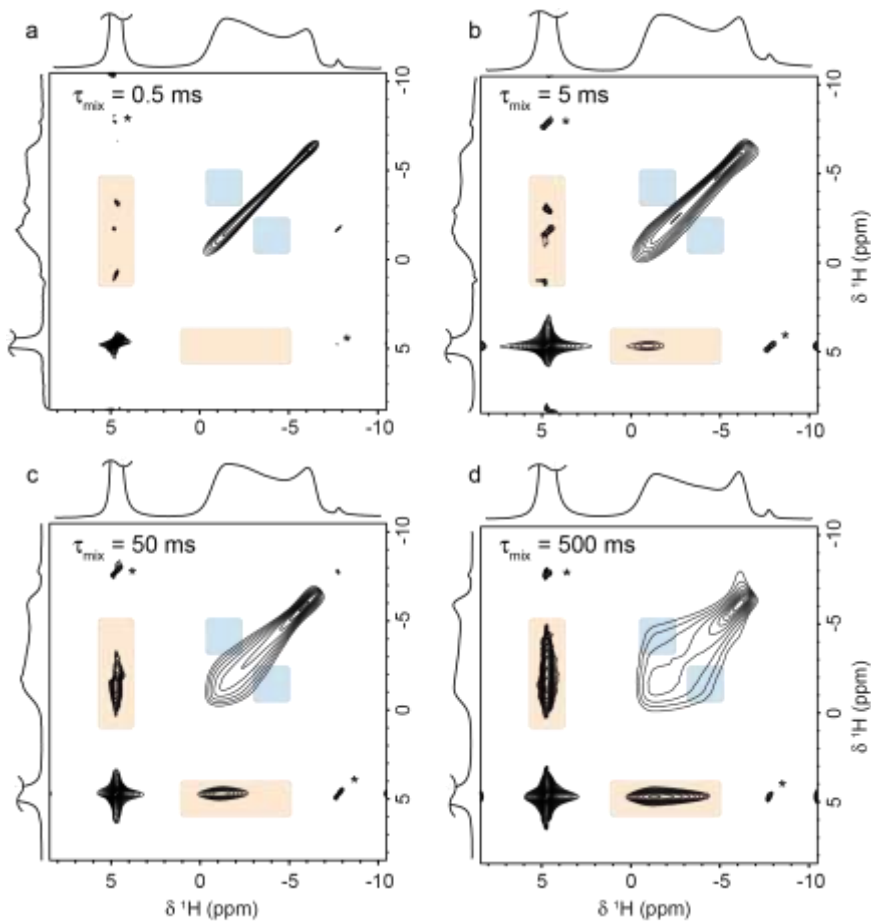


**Figure 2:**  $^1\text{H}$  MAS exchange NMR spectra with mixing times of (a) 0.5 ms, (b) 5 ms, (c) 50 ms and (d) 500 ms using 15 mg of PDC with burn-off 45 % saturated with 15  $\mu\text{L}$  of deionised  $\text{H}_2\text{O}$ . Highlighted areas indicate where cross-peaks are expected for in-pore – ex-pore exchange (orange) and in-pore – in-pore exchange (blue). Spinning sidebands are denoted by asterisks.

timescale between species adsorbed in the largest pores and those in the bulk solution. For  $\tau_{\text{mix}} = 50 - 500$  ms, (Figures 2c,d) broadening of the diagonal in-pore resonance also signifies exchange between pores of different sizes. Overall these observations show that the steam activation process results in particles with different average pore sizes, including some particles or regions of particles

that remain unactivated (as shown by the remaining in-pore resonance at  $\delta = -6$  ppm). The adsorbed  $H_2O$  molecules undergo interparticle exchange whereby they first exchange with the bulk solution before exchanging with pores of different sizes in other particles. We note that even with a mixing time of 500 ms, no exchange was observed involving the unactivated pores at  $\delta = -6$  ppm, indicating that diffusion within these subnanometre pores is severely restricted and  $H_2O$  molecules adsorbed within them remain effectively isolated from the rest of the porous network.

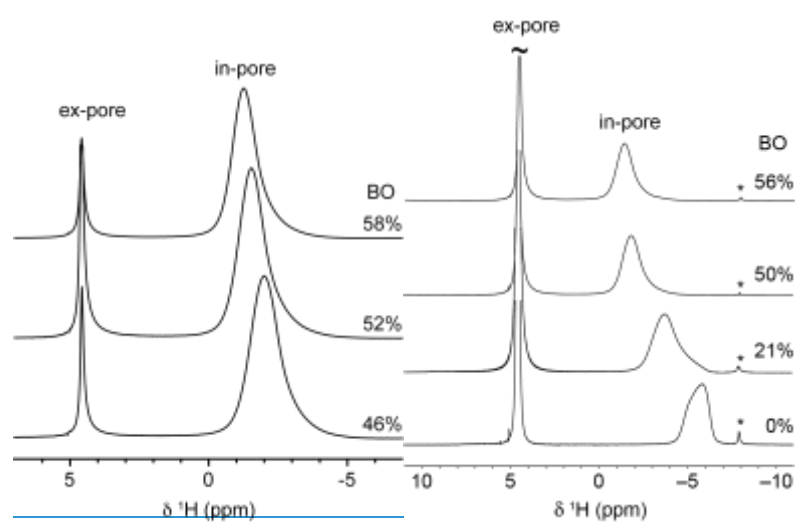


**Figure 3:**  $^1H$  MAS NMR spectra of PDC samples which were sieved prior to the steam activation process and saturated with deionised  $H_2O$ . Asterisks denote spinning sidebands.

that remain unactivated (as shown by the remaining in-pore resonance at  $\delta = -6$  ppm). The adsorbed  $H_2O$  molecules undergo interparticle exchange whereby they first exchange with the bulk solution before exchanging with pores of different sizes in other particles. We note that even with a mixing time of 500 ms, no exchange was observed involving the unactivated pores at  $\delta = -6$  ppm, indicating that diffusion within these subnanometre pores is severely restricted and  $H_2O$  molecules adsorbed within them remain effectively isolated from the rest of the porous network.

A likely reason for the pore structure inhomogeneity is the large particle size distribution obtained when the carbonised PEEK is manually crushed prior to steam activation (see Supporting Information). In an effort to reduce the particle size distribution, the crushed carbonised PEEK was passed through a sieve of mesh size 62  $\mu\text{m}$  prior to steam activation. Following this procedure, the modal particle size was found to be 92  $\mu\text{m}$ , with 98% of the carbon particles were found to have having a diameter of less than 200  $\mu\text{m}$  as measured by DLS analysis (see Supporting Information). As a precautionary measure during activation, the humidity was also controlled by fixing the gas flow rate in the furnace tube to  $0.5 \text{ L min}^{-1}$  and the water temperature within the Dreschel bottle to  $30^\circ\text{C}$ . The sample was also spread with a uniform layer thickness on the surface of an inverted alumina boat to minimize turbulence. Figure 3 shows  $^1\text{H}$  MAS NMR spectra of PDCs prepared in this way and saturated with deionised  $\text{H}_2\text{O}$ . In comparison to the unsieved PDCs, these spectra exhibit much narrower and more

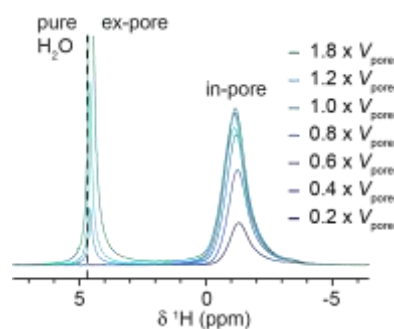


**Figure 4:**  $^1\text{H}$  MAS NMR spectra of sieved PDC with BO = 62% soaked with increasing amounts of deionised  $\text{H}_2\text{O}$  relative to the total pore volume as measured by gas sorption ( $V_{\text{pore}}$ ).

tube to  $0.5 \text{ L min}^{-1}$  and the water temperature within the Dreschel bottle to  $30^\circ\text{C}$ . The sample was also spread with a uniform layer thickness on the surface of an inverted alumina boat to minimize turbulence. Figure 3 shows  $^1\text{H}$  MAS NMR spectra of PDCs prepared in this way and saturated with deionised  $\text{H}_2\text{O}$ . The BO = 0% sample shows no change from the unsieved PDC showing that the intrinsic porosity following carbonisation is not altered by the sieving process. However, in

~~comparison to the unsieved PDCs, the spectra of the sieved PDCs exhibit much narrower and more symmetric in-pore resonances with~~  
~~no very little~~ evidence of the  $\delta = -6$  ppm resonance corresponding to ~~the~~ unactivated pores. This confirms that the steam-activation process is particle size-dependent, and therefore that careful control over the particle size is important in order to achieve a homogeneously activated sample.

For the sieved PDCs, the increased resolution of the in-pore resonance ~~enables the NICS to be measured more accurately.~~ ~~allows the NICS to be measured more accurately and its magnitude interpreted in more detail.~~ It can be seen that the NICS reduces with increasing burn-off, which is consistent with previous studies on PDCs and has been interpreted in terms of increasing pore size.[35] However, another factor that could potentially influence the NICS is exchange between in-pore species and species located near the particle surface or in the ex-pore environment, as demonstrated recently by Fulik *et al.* In the limit of fast in-pore – ex-pore exchange, the in-pore resonance will be observed at the average between the true NICS and the ex-pore chemical shift, weighted by the size of the subpopulation of ex-pore species that are involved in the exchange process.[39] In the case of intermediate exchange (when the exchange rate is comparable to the absolute frequency difference of the in-pore and ex-pore environments), smaller changes in the NICS can also be observed, together with line broadening effects. Exchange effects are most evident when comparing NMR spectra of samples with and without excess free liquid, whereby a reduction in the apparent NICS is observed upon saturation of the sample due to the onset of the exchange process. To investigate the possibility of such effects, NMR spectra were recorded for a sieved PDC sample with BO = 62% which was soaked with increasing volumes of H<sub>2</sub>O (Figure 4). At loadings significantly lower than the total pore volume  $V_{\text{pore}}$  (as determined by gas sorption measurement), the in-pore resonance is observed at -1.3 ppm. As the loading is increased, an ex-pore resonance appears at 4.6 ppm when the injected volume equals the total pore volume. At this point and also at higher loadings, very little change is observed in the shift of the in-pore resonance, and the shift of the ex-pore resonance is very close to that for bulk H<sub>2</sub>O (4.8 ppm). This suggests that exchange between in-

pore and ex-pore species is slower than the NMR timescale in this experiment and does not significantly affect the NICS in this system. To investigate this further, exchange experiments were performed on a sieved PDC sample with BO = 57% (Figure 5). At a short  $\tau_{\text{mix}}$  of 0.6 ms (Figure 5a), no significant in-pore – ex-pore exchange is observed and the in-pore resonance is confined to the diagonal line indicating that its width is again inhomogeneous in origin a distribution of pore environments. For a longer  $\tau_{\text{mix}}$  of 50 ms (Figure 5b), in-pore – ex-pore cross peaks are observed, showing that exchange takes place on this timescale.

To gain more quantitative insight into the exchange processes present, cross-peak intensities were extracted from exchange spectra recorded for  $\tau_{\text{mix}}$  between 0 – 600 ms. In principle, the rate constant of a two site exchange process,  $k$ , can be determined from the build up of the integrated intensity ratio of cross peaks and diagonal peaks ( $I_{\text{cross}} / I_{\text{diag}}$ ) as a function of  $\tau_{\text{mix}}$ . However, as found in previous work,[27, 39] a poor fit was obtained when the expected dependence on  $\tanh(k\tau_{\text{mix}})$  was assumed.

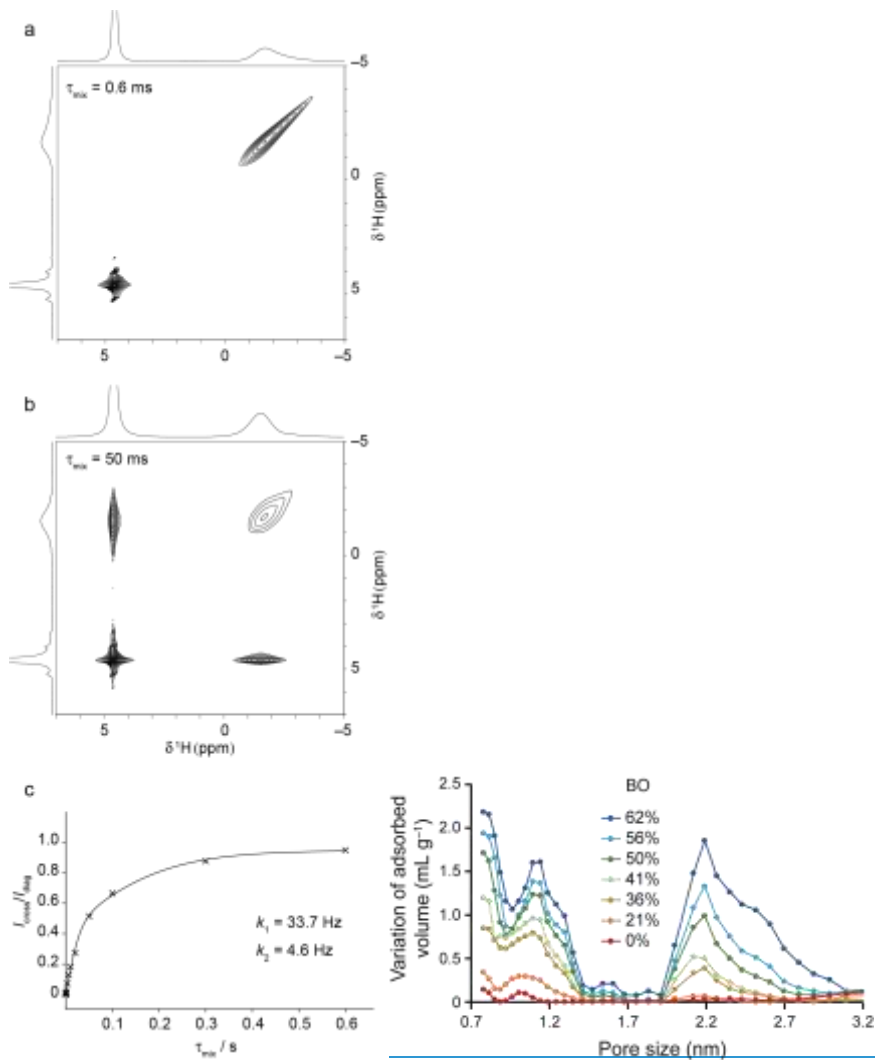


Figure 5:  $^1\text{H}$  MAS exchange NMR spectra of sieved PDC with BO = 57% with mixing times of (a) 0.6 and (b) 50 ms. (c) Plot of the ratio of cross-peak and diagonal peak intensities ( $I_{\text{cross}}/I_{\text{diag}}$ ) as a function of mixing time in the exchange experiments.

Figure 4: Plot of differential pore volume between 0.8 and 3.0 nm for PDC samples with burn-offs between 0–62%. All samples were sieved prior to steam activation as described in the main text.

Formatted: Centered

Formatted: Not Highlight

Formatted: Font: Italic

Formatted: Subscript

Formatted: Font: Italic

Formatted: Subscript

size.[35] [39] Indeed, Fulik *et al.* showed that a better fit could be obtained assuming the presence of two exchange processes characterised by different rate constants corresponding to in-pore – ex-pore exchange near the surfaces of the carbon particles ( $k_1$ ), and the diffusion of in-pore species from the centre of the particles to the surface ( $k_2$ ).[39] In this case,  $I_{cross} / I_{diag}$  is described by:

$$I_{cross}/I_{diag} = A \tanh(k_1 \tau_{mix}) + B \tanh(k_2 \tau_{mix}) \quad (1)$$

As shown in Figure 5c, Eq. (1) gives a good fit to the experimental data, yielding values of  $A = 0.43$ ;  $B = 0.51$ ;  $k_1 = 33.7$  Hz and  $k_2 = 4.6$  Hz. However, we note that the rate constants obtained are significantly smaller than those previously determined by Fulik *et al.* for organic electrolytes in a commercial microporous carbon.[39] This may be partly attributed to the different chemical properties of the H<sub>2</sub>O molecules studied here, although we note that the diffusion coefficients of unconfined H<sub>2</sub>O species (*vide infra*) are comparable with organic electrolyte species to within an order of magnitude.[69] A more important factor is likely to be the relatively large carbon particle size used in our experiments. As mentioned above, the modal particle size of the sieved PDC particles is 92  $\mu\text{m}$  which is nearly two orders of magnitude larger than the particle size of the commercial carbon used in the previous study. This means that the interfacial region where fast in-pore – ex-pore exchange takes place across the surface of the particles is much smaller compared to the interior volume of the particles, and therefore diffusion processes within the particles (*i.e.*, fast exchange between pores of different sizes) should be the dominant factor in controlling the overall in-pore – ex-pore exchange process. Because the interfacial region is so small, the slow timescale intraparticle diffusion process effectively masks the contribution from the faster in-pore – ex-pore exchange process at the particle surface. Indeed, as shown in Supporting Information, in contrast to the previous study by Fulik *et al.* the results from the exchange experiments do not show a clear distinction between a fast timescale exchange process at sub-millisecond  $\tau_{mix}$  and a much slower process at longer

$\tau_{\text{mix}}$ . Therefore, rather than parameterising the interfacial in-pore – ex-pore exchange process, the  $k_1$  value obtained from our fit most likely encompasses a more complex exchange process within a larger

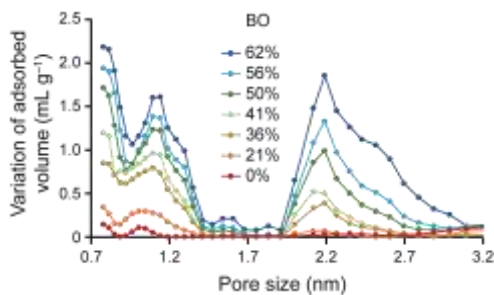


**Figure 6:** Plot of differential pore volume between 0.8 and 3.0 nm for PDC samples with burn-offs between 0 – 62%. All samples were sieved prior to steam activation as described in the main text.

interior region near the particle surface which is not fully decoupled from the much slower intraparticle diffusion kinetics.

Overall, the saturation build-up and exchange experiments show that the overall in-pore - ex-pore exchange kinetics are significantly reduced in the sieved PDCs due to the large particle size. In the absence of significant exchange effects, it should therefore be possible to investigate the influence of the carbon pore structure on the NICS through comparison of PDCs with different burn-offs. To further investigateAs an independent probe of the evolution of the pore structure with burn-off, gas sorption measurements were carried out on PDCs with BO values in the range 0 – 62%. Pore size distributions between 0.8 – 3.2 nm are shown in Figure 6. Measurements between 3 - 30 nm did not show any significant porosity, confirming that the PDCs are predominantly microporous (see Supporting Information). The gas sorption results show that in general the PDCs exhibit a trimodal pore size distribution comprising a subnanometre pore population around 0.8 nm, a second pore population centred around 1.1 nm and a broader distribution in the range 2 – 3 nm. We note that these pore widths are approximately equal to integer multiples of the layer spacing in graphite and may suggest an activation mechanism relating to etching of individual sheets within locally ordered

graphitic domains in the carbonised material (see Supporting Information). However, these results also show that the pore sizes within each sub-population do not change significantly with increasing burn-off; instead, the relative proportions of pore sizes within each sub-population vary, with increasing porosity in the 2 – 3 nm range for higher burn-offs. This agrees with previous gas sorption measurements on PDCs[31, 42] and highlights an important distinction when using the NICS as a probe of the carbon pore structure. In principle, H<sub>2</sub>O molecules adsorbed in different sized pores should exhibit different NICSs, resulting in multiple in-pore resonances in the NMR spectrum. However, as seen in Figure 3, only a single in-pore resonance is observed for each BO value. This is explained by the fact that at ambient temperature the water molecules are highly mobile within the

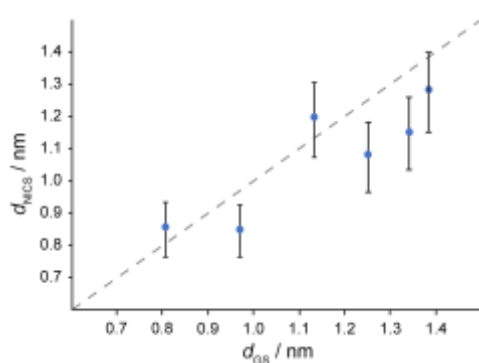


**Figure 5:** Comparison of the average pore size derived from the NICS of in-pore H<sub>2</sub>O species,  $d_{NICS}$ , and from gas sorption measurements,  $d_{GS}$ , for different PDC samples. The dotted line represents perfect agreement. Error bars are derived from the full width at half maximum of the in-pore resonance.

only a single in-pore resonance is observed for each BO value. This is explained by the fact that at ambient temperature the water molecules within the pore structure ~~and~~ undergo intraparticle exchange between the different pore environments on a timescale that is faster than the NICS frequency differences.[39] As a result, a single resonance is observed with a NICS corresponding to the average pore size. Therefore although the individual pore sizes do not change significantly with burn-off, the

Formatted: Centered

increase in the relative proportion of mesopores causes the average pore size to increase, resulting in a reduction in the NICS.

[27, 39][27, 39][39][39][69]

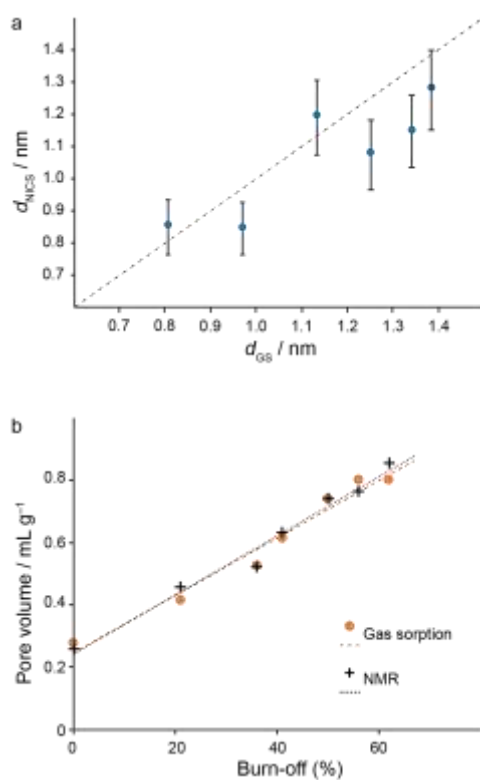


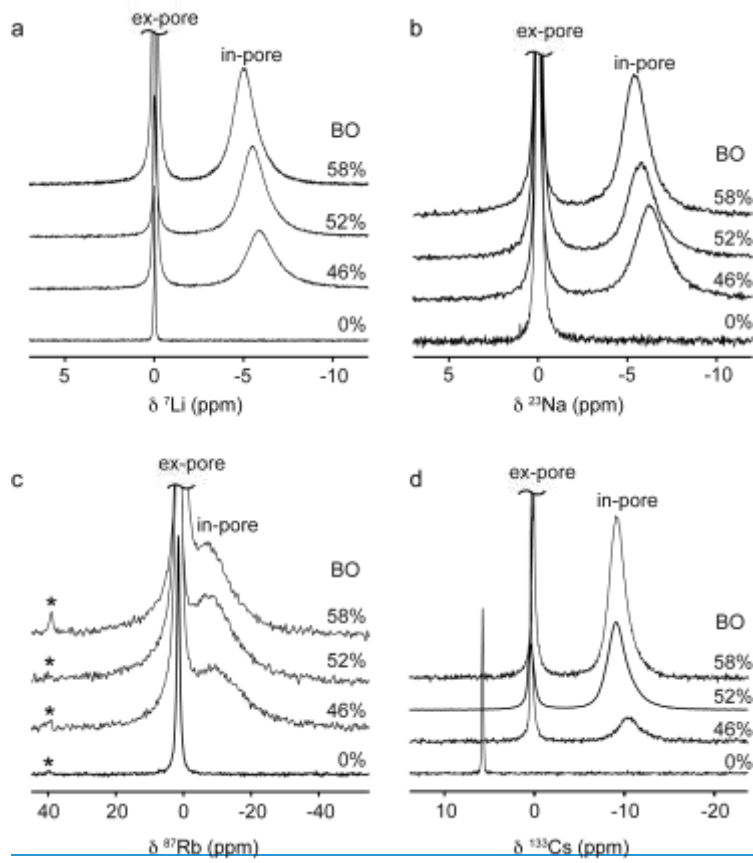
**Figure 7:** (a) Comparison of the average pore size derived from the NICS of in-pore H<sub>2</sub>O species,  $d_{NICS}$ , and from gas sorption measurements,  $d_{GS}$ , for different PDC samples. The dotted line represents perfect agreement. Error bars are derived from the full width at half maximum of the in-pore resonance. (b) Comparison of total pore volume determined by NMR (crosses) and gas sorption (circles). Dotted and dashed lines represent best fits to the two datasets.

circumcoronene molecules. If the local domain size or curvature within the PDCs differs significantly from this, it would lead to be a systematic discrepancy between  $d_{NICS}$  and  $d_{GS}$ . As a further probe of

[the pore structure, we also compared the total pore volume for PDCs determined from gas sorption with that determined from the integrated intensity of the in-pore resonance as a fraction of the total amount of liquid added to the sample. As shown in Figure 7b, a strong linear relationship between burn-off and total pore volume is observed, and very good agreement is obtained from the two measurements. This confirms that NMR serves as a very useful probe of the pore volume in microporous carbon materials. Also we note that the good agreement with the gas sorption pore volume is also evidence that in-pore – ex-pore exchange effects are not significant in these systems. In the fast exchange limit, the intensities of the in-pore and ex-pore resonances should be modified to account for the proportion of each population that is undergoing exchange. If this was the case, the integrated intensity of the in-pore resonance would not reflect the true proportion of species in the in-pore environment and poor agreement with the gas sorption data would be expected.](#)

**Specific Ion Effects.** One of the advantages of using alkali metal chloride electrolytes as a model system is that all the stable cationic nuclei in this group except potassium are readily observable by NMR spectroscopy, allowing a systematic comparison. Figure 86 shows  $^7\text{Li}$ ,  $^{23}\text{Na}$ ,  $^{87}\text{Rb}$  and  $^{133}\text{Cs}$  MAS NMR spectra of PDCs with burn-offs in the range 0 - 58% saturated with the corresponding aqueous alkali metal chloride solution at 1 M concentration. For all cations, no in-pore resonances are observed for PDCs with 0% burn-off. This suggests that although the inherent porosity in the carbonised material is accessible to  $\text{H}_2\text{O}$  molecules (Figure 86a), the cations are too large to enter in a hydrated or partially hydrated state. We note that for  $^{133}\text{Cs}$ , the chemical shift of the ex-pore resonance for the PDC with 0% burn-off differs by approximately 0.86 ppm compared to the other salt solutions. This is attributed to the strong concentration dependence of the  $^{133}\text{Cs}$  chemical shift which is well known[70, 71] (see Supporting Information). For this sample, the selective adsorption of  $\text{H}_2\text{O}$  molecules increases the ex-pore concentration and shifts the  $^{133}\text{Cs}$  resonance to higher chemical shift. [Based on a chemical shift calibration for known concentrations \(see Supporting Information\), the 0.8 ppm shift corresponds to the ex-pore solution having a concentration of 1.1 M.](#)

This compares to 1.3 M as determined from the ratio of in-pore and ex-pore  $^1\text{H}$  resonance integrals for the same sample. It is possible that the small discrepancy between these values is due to a small proportion of the  $\text{Cs}^+$  ions becoming immobilised upon entry to the pores (due the very small pore width in this sample), in which case these would not For the steam-activated PDCs, in-pore resonances are observed for each salt solution, with NICSs that decrease with increasing burn-off. Since only a single in-pore resonance is observed for each system, this shows that (like the  $\text{H}_2\text{O}$  molecules) the in-pore cations also undergo fast exchange between the different micropore environments, and the observed NICS is a reflection of the exchange-averaged pore size. We note that in the  $^{87}\text{Rb}$  MAS NMR spectra much larger in-pore linewidths are observed, which extend far outside the typical NICS range. In this case, rather than relating to the structure of the carbon or cation behaviour, the large linewidth is attributed to fast quadrupolar relaxation due to the large quadrupole moment of this nucleus. [72]



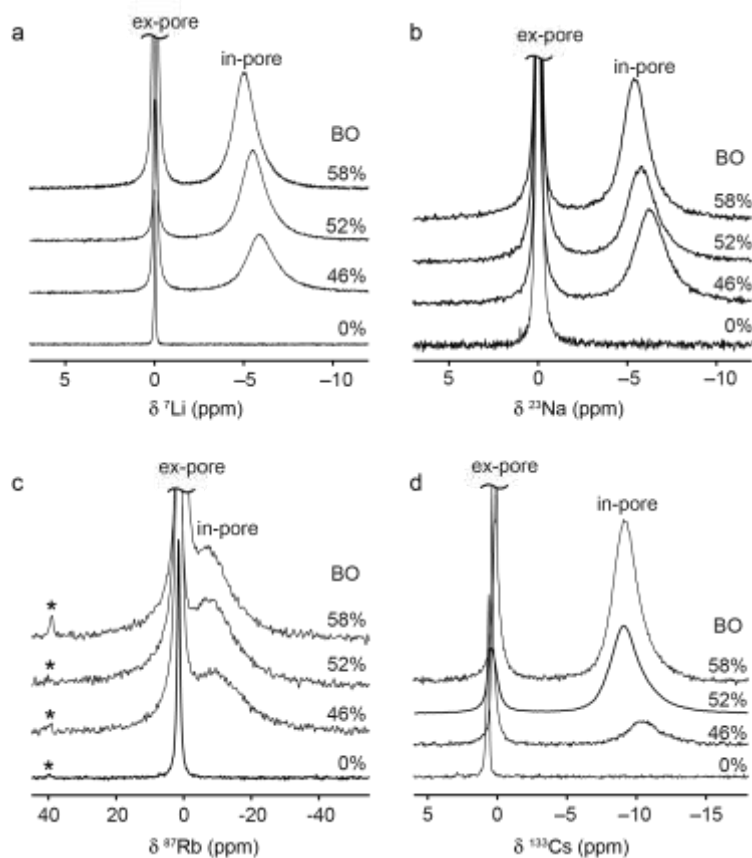


**Figure 86:** MAS NMR spectra of PDC samples saturated with 1 M aqueous solutions of (a) LiCl, (b) NaCl, (c) RbCl and (d) CsCl.

be observed due to considerable quadrupolar and chemical shift anisotropy broadening. In this case the ex-pore concentration would be overestimated by the integral method.

For the steam-activated PDCs, in-pore resonances are observed for each salt solution, with NICSs that decrease with increasing burn-off. Since only a single in-pore resonance is observed for each system, this shows that (like the H<sub>2</sub>O molecules) the in-pore cations also undergo fast exchange between the different micropore environments, and the observed NICS is a reflection of the exchange-

behaviour, the large linewidth is attributed to fast quadrupolar relaxation due to the large quadrupole moment of this nucleus.[72]

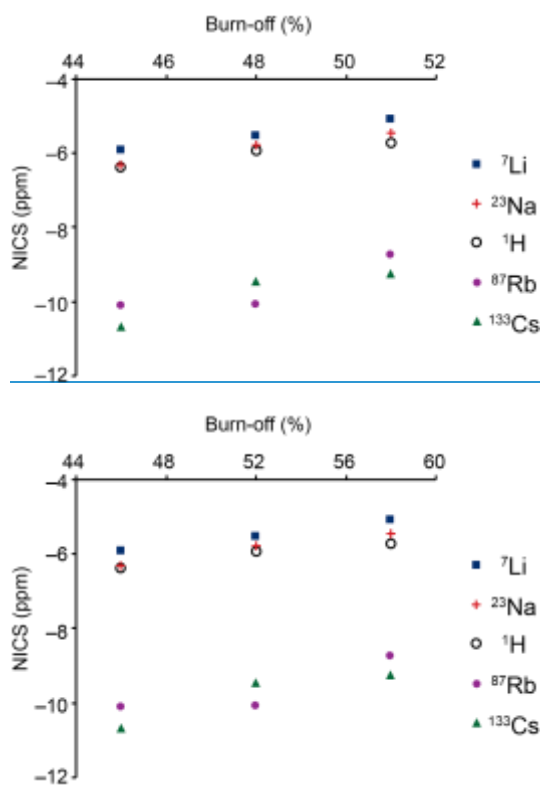


**Figure 97:** Plot of NICS as a function of burn-off for saturated PDC samples. NICSs for cationic species were obtained from MAS NMR measurements on PDCs saturated with the corresponding 1 M aqueous chloride solution while the <sup>1</sup>H NICS values were obtained from PDC samples soaked with deionised H<sub>2</sub>O.

averaged pore size. We note that in the <sup>87</sup>Rb MAS NMR spectra much larger in-pore linewidths are observed, which extend far outside the typical NICS range. In this case, rather than relating to the structure of the carbon or cation behaviour, the large linewidth is attributed to fast quadrupolar relaxation due to the large quadrupole moment of this nucleus.[72]

~~In previous work on the adsorption of aqueous NaBF<sub>4</sub> in PDCs, similar NICSs were observed for all adsorbed species within a particular type of PDC.[35] However, for the aqueous alkali metal chlorides, the NICSs differ significantly for the different cationic species. This is illustrated in Figure 9 which compares the magnitude of the NICS observed for each nucleus with that of pure H<sub>2</sub>O in each of the steam-activated PDCs. Compared to <sup>1</sup>H, the <sup>23</sup>Na and <sup>7</sup>Li NICSs are slightly smaller for each burn-off value whereas the <sup>87</sup>Rb and <sup>133</sup>Cs NICS are markedly larger by 4 -5 ppm. larger. Since all experiments were performed using PDCs with similar ~100 μm particle sizes, it is unlikely that the larger NICS of <sup>87</sup>Rb and <sup>133</sup>Cs is related to in-pore – ex-pore exchange phenomena. Furthermore, the build-up experiment and exchange spectra in the previous section confirm that the <sup>1</sup>H NICS is not significantly affected by exchange. If for some reason Rb<sup>+</sup> and Cs<sup>+</sup> had dramatically different help rationalise these differences, molecular dynamics simulations were performed to estimate effective hydrated diameters for the alkali metal cations in aqueous solution. K<sup>+</sup> was included in the simulations for completeness although the low sensitivity of this nucleus precluded its observation in the NMR experiments. Figure 8 shows radial distribution functions (RDFs) averaged over 17.5 ps for each simulation. For each cation there is clear evidence of a structured hydration shell as indicated by the maxima in the RDFs corresponding to cation – oxygen distances, with a trend in increasing radius from 2.0 Å for Li<sup>+</sup> to 3.2 Å for Cs<sup>+</sup>. However, Li<sup>+</sup> and Na<sup>+</sup> also show strong evidence of a second hydration shell with additional maxima at approximately 4.0 and 4.5 Å, respectively. Therefore, while Rb<sup>+</sup> and Cs<sup>+</sup> have larger ionic radii, in terms of the effective hydrated ion size, Li<sup>+</sup> and Na<sup>+</sup> are the largest species. In contrast to the H<sub>2</sub>O molecules which are free to exchange between all positions within the pore, the large and strongly bound hydration shells of Li<sup>+</sup> and Na<sup>+</sup> prevent direct coordination with the pore walls meaning that on average these ions reside further from the carbon surface and therefore exhibit a reduced NICS. Conversely, the smaller hydration shells of Rb<sup>+</sup> and Cs<sup>+</sup> means they can more closely approach the carbon surface and experience enhanced NICS. In addition, the fact that Rb<sup>+</sup> and Cs<sup>+</sup> are much less strongly hydrated means they are more prone to~~

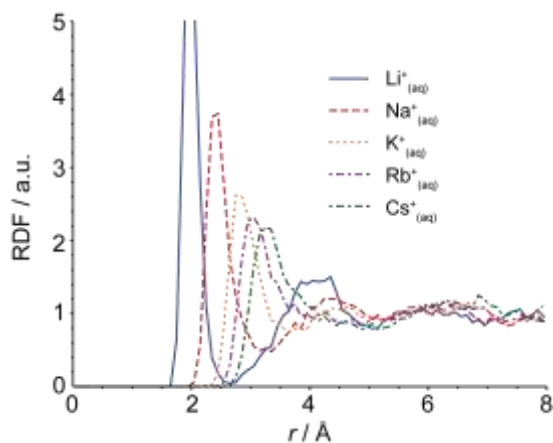


**Figure 108:** Radial distribution functions averaged over 17.5 ps *ab initio* molecular dynamics simulations for alkali metal ions in aqueous solution.

exchange properties, the NICS for these nuclei should be reduced rather than increased. Therefore, to help rationalise the NICS differences, molecular dynamics simulations were performed to estimate effective hydrated diameters for the alkali metal cations in aqueous solution.  $K^+$  was included in the simulations for completeness although the low sensitivity of this nucleus precluded its observation in the NMR experiments. Figure 10 shows radial distribution functions (RDFs) averaged over 17.5 ps for each simulation. For each cation there is clear evidence of a structured hydration shell as indicated by the maxima in the RDFs corresponding to cation - oxygen distances, with a trend in increasing radius from 2.0 Å for  $Li^+$  to 3.2 Å for  $Cs^+$ . However,  $Li^+$  and  $Na^+$  also show strong evidence of a second hydration shell with additional maxima at approximately 4.0 and 4.5 Å, respectively. Therefore, while  $Rb^+$  and  $Cs^+$  have larger ionic radii, in terms of the effective hydrated ion size,  $Li^+$  and  $Na^+$  are the largest species. In contrast to the  $H_2O$  molecules which are free to exchange between all positions within the pore, the large and strongly bound hydration shells of  $Li^+$  and  $Na^+$  prevent direct coordination with the pore walls meaning that on average these ions reside further from the carbon surface and therefore exhibit a reduced NICS. Conversely, the smaller hydration shells of  $Rb^+$  and  $Cs^+$  means they can more closely approach the carbon surface and experience enhanced NICS. In addition, the fact that  $Rb^+$  and  $Cs^+$  are much less strongly hydrated means they are more prone to

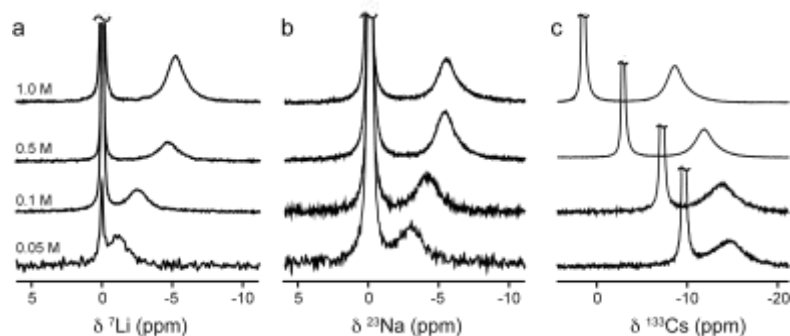


**Figure 119:** (a)  $^7\text{Li}$ , (b)  $^{23}\text{Na}$  and (c)  $^{133}\text{Cs}$  MAS NMR spectra of PDC samples soaked with the corresponding aqueous chloride solution at concentrations between 0.05 – 1 M. The burn-off was (a) 53% and (b, c) 56%.

[distortion and partial dehydration as they approach pore walls. DFT calculations have shown that the removal of water molecules from the coordination shells of hydrated ions leads directly to a significant increase in chemical shielding by several ppm.\[45, 73\] Although the physical origin of this shift is different to the ring current-induced NICS, both effects result in a shift to high field in the NMR spectrum, and therefore combine to increase the apparent magnitude of the NICS.](#)

**Concentration Effects.** [The comparison of NMR spectra for the different aqueous solutions reveals how specific ion effects can influence the shift of the in-pore species. However, NMR spectra recorded for PDCs saturated with solutions of different concentrations, shown in Figure 11, reveal an additional concentration dependence. As the concentration of the injected electrolyte is reduced from 1 M to 0.05 M, the NICS reduces significantly by up to 4.9 ppm \(for Cs there is an additional shift due to the concentration dependence of the chemical shift\). Fulik \*et al.\* have reported similar effects for  \$\text{BF}\_4^-\$  species in organic electrolytes adsorbed on microporous carbons.\[39\] Although the origin of the concentration effect was not conclusively determined, in the systems studied exchange effects on the NICS were shown to be significant. To test if the concentration dependence observed in the current work is related to exchange effects, of the ex-pore species close to the carbon particles. This](#)

saturation NICS is  $-6.0$  ppm and this reduces by  $0.4$  ppm upon saturation of the sample. For  $0.1$  M

and  $0.1$  M NaCl. For  $1$  M NaCl (Figure 120a), the pre-saturation NICS is  $-6.0$  ppm and this reduces by  $0.4$  ppm upon saturation of the sample. For  $0.1$  M

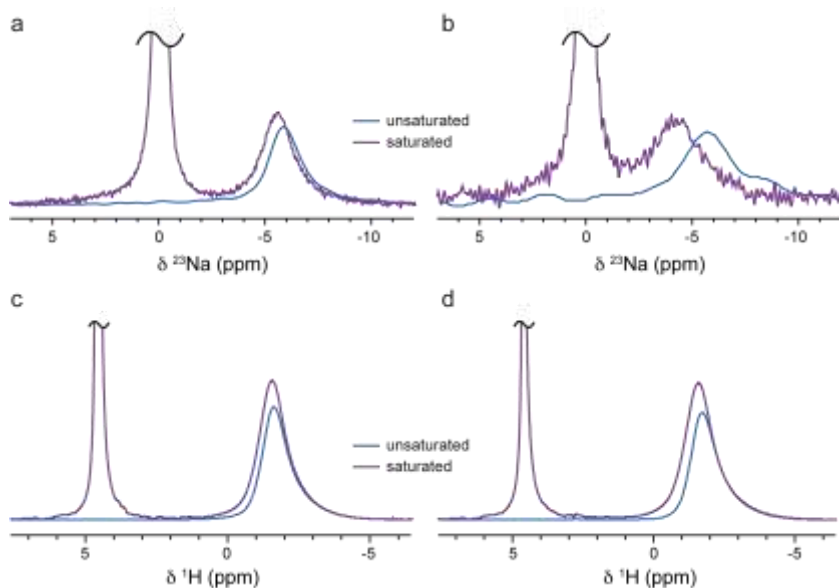


**Figure 120:** (a, b)  $^{23}\text{Na}$  and (c, d)  $^1\text{H}$  MAS NMR spectra of a PDC with burn-off 53% loaded with (a, c)  $1$  M and (b, d)  $0.1$  M  $\text{NaCl}_{(\text{aq})}$ . Spectra are shown before saturation (blue line) and after saturation (purple line).

**Table 1.** Diffusion coefficients ( $\text{m}^2 \text{s}^{-1}$ ) for  $\text{H}_2\text{O}$  and cationic species in aqueous salt solutions at  $0.1$  M and  $1$  M concentration.

	LiCl		NaCl		CsCl	
	$D_{\text{H}_2\text{O}}$	$D_{\text{Li}^+}$	$D_{\text{H}_2\text{O}}$	$D_{\text{Na}^+}$	$D_{\text{H}_2\text{O}}$	$D_{\text{Cs}^+}$
$0.1$ M	$2.28 \times 10^{-9}$	$1.02 \times 10^{-9}$	$2.30 \times 10^{-9}$	$0.58 \times 10^{-9}$	$2.30 \times 10^{-9}$	$0.23 \times 10^{-9}$
$1$ M	$2.06 \times 10^{-9}$	$0.93 \times 10^{-9}$	$2.17 \times 10^{-9}$	$0.57 \times 10^{-9}$	$2.40 \times 10^{-9}$	$0.23 \times 10^{-9}$

saturation NICS is  $-6.0$  ppm and this reduces by  $0.4$  ppm upon saturation of the sample. For  $0.1$  M NaCl, (Figure 12b) the NICS reduces by a larger value of  $1.65$  ppm upon saturation. At first sight, this is consistent with exchange averaging of the NICS in the  $0.1$  M sample. However, it is important to note that  $^1\text{H}$  MAS NMR spectra of the same samples (Figures 12c,d) show almost no change in the

NICS for both concentrations. Based on the exchange-averaging hypothesis, this would imply that the H<sub>2</sub>O molecules are significantly less mobile than the Na<sup>+</sup> ions in the 0.1 M electrolyte. To quantify the relative mobilities of the Na<sup>+</sup> and H<sub>2</sub>O species, NMR diffusion measurements were carried out on neat solutions. The diffusion coefficients, summarised in Table 1, show that the average mobility of the H<sub>2</sub>O molecules is approximately a factor of 4 higher than the cations in the same solution, so assuming exchange averaging alone, similar NICS reductions should be observed for both species. Moreover, no difference in the Na<sup>+</sup> diffusion coefficient is measured within experimental error between the 1 M and 0.1 M solutions. Although the ion mobility inside the micropores is expected to be lower than in the neat solution, similar exchange effects should be expected for both concentrations. These results suggest ~~that~~ the concentration difference does not significantly affect the ion mobility, and therefore in-pore – ex-pore exchange averaging does not fully explain the observed reduction in the NICS at low concentration.

An alternative explanation is that the NICS reduction arises from a redistribution of the in-pore ions within the porous network, with favoured occupancy of larger pores at low concentrations. This would cause the ions to reside further from the surface on average, resulting in a reduction in the NICS due to the distance dependence. Indeed, favoured occupancy of larger pores should be expected based on a number of theoretical studies that predict significant energy barriers (or positive adsorption energies) for the entry of hydrated ions to micropores.[9, 11-14, 74] In these studies, the positive adsorption energy has been found to depend mainly upon the relative sizes of the pore and the hydrated ion. Therefore, in PDCs which contain a distribution of pore sizes there will be a distribution of adsorption energies, and at thermal equilibrium pores of different widths will be occupied according to Boltzmann statistics. The precise distribution of ions across different pore widths will depend upon the balance between the adsorption energies for each pore and the chemical potential of the electrolyte ions. However, reducing the electrolyte concentration reduces the chemical potential of the ions, which should result in a redistribution of the ions between different pore sizes, with

occupancy of larger pores becoming more favoured in order to minimise the total energy of the system. Since the NICS corresponds to the average pore size that the ions explore, reduced occupation of smaller micropores and increased occupation of larger micropores should lead to a reduction in the NICS.

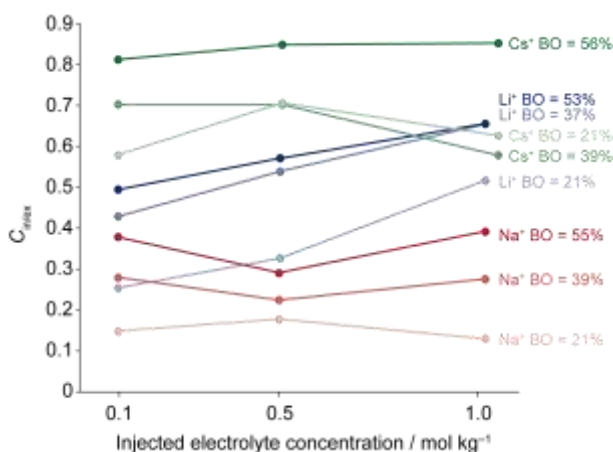


**Figure 13:**  $C_{in}/C_{ex}$  for LiCl (blue), NaCl (red) and CsCl (green) salt solutions as a function of injected electrolyte concentration and for PDCs with different BO values. Straight lines joining points are shown as a guide to the eye. Error bars have been omitted for clarity but were less than 15% in all measurements.

of smaller micropores and increased occupation of larger micropores should lead to a reduction in the NICS.

It is difficult to test this hypothesis directly as it is not possible to determine the local ion concentrations in pores of different widths due to fast exchange averaging between the different pore environments. However, insight can be gained from the average in-pore and ex-pore ion concentrations which are determined from the relative resonance intensities of cation and H<sub>2</sub>O species in the NMR spectra (see Experimental Details). Based on the assumption of a positive adsorption energy, the average in-pore concentration is expected to be lower than the ex-pore concentration at thermal equilibrium. This is exactly what is observed in Figure 13 which shows the ratio of in-pore and ex-pore concentrations,  $C_{in}/C_{ex}$ , as a function of the neat electrolyte concentration in PDCs with

low, intermediate and high burn-off. For all electrolytes,  $C_{in}/C_{ex}$  is lower than 1, showing that the average in-pore concentration is suppressed compared to the ex-pore electrolyte. Similar results were observed in previous work by Luo *et al.*, where in-pore  $Na^+$  concentrations in PDCs were reduced for a range of aqueous Na-based electrolytes.[44] In that work, the in-pore cation concentration was found to be strongly affected by the nature of the anion. In the current work, the same chloride anion is used in all cases, and therefore differences in the in-pore cation concentration should reflect specific ion properties of the cations themselves. In general  $C_{in}/C_{ex}$  is lowest for  $Na^+$  which has the largest hydrated ion size and a strongly-held hydration shell, intermediate for  $Li^+$ , and highest for  $Cs^+$  which is the smallest ion with the greatest propensity for desolvation. This is consistent with strongly solvated ions being energetically

Additional insight can be obtained by comparing the  $C_{in}/C_{ex}$  values for each ion as a function of concentration. ~~If the reduction in the NICS at low concentration was due to exchange averaging,  $C_{in}/C_{ex}$  would be expected to increase to reflect the contribution of the subset of exchanging ex-pore ions to the intensity of the exchange averaged in-pore resonance. However, this is not observed~~ in Figure 134; ~~instead~~  $C_{in}/C_{ex}$  remains approximately constant for  $Na^+$  and  $Cs^+$  and ~~even~~ reduces slightly for  $Li^+$  across the concentration range studied. This means that as the injected electrolyte concentration is reduced, the equilibrium in-pore concentration also reduces by a similar amount. The concomitant reduction in the ~~number of~~ in-pore ionspecie populations with the neat electrolyte concentration ~~is further evidence that in-pore ex-pore exchange averaging is not the primary cause of the NICS reduction at low concentration. It~~ suggests that the in-pore population is largely dependent on the balance between the chemical potential of the ex-pore electrolyte ions and the positive adsorption energies of the pores in the PDC structure. As the concentration is reduced, the difference between the positive adsorption energy and the chemical potential of the electrolyte ions increases, forcing the ions out of the smallest pores and into the bulk electrolyte solution until a new balance is achieved.

It is possible to gain qualitative insight into the local adsorption energies associated with different pore sizes by comparing  $C_{in/ex}$  values for PDCs with different burn-offs. Figure 11 shows that in general for each of the cations studied,  $C_{in/ex}$  increases with increasing burn-off. Based on the gas sorption data in Figure 64, PDCs with higher burn-off contain higher relative proportions of mesopores in the 2 – 3 nm range (see also Supporting Information). The increase in  $C_{in/ex}$  with burn-off therefore suggests that the introduction of a higher proportion of mesopores enables the porous network to accommodate higher concentrations of ions. This supports the expectation from theoretical studies that mesopores should provide lower energy adsorption sites than micropores, thereby allowing greater equalisation of the in-pore and ex-pore concentrations. This also further implies that reducing the total electrolyte concentration should result in a redistribution of the in-pore ions between the micropore and mesopore environments to minimise the total energy of the system.

While it is not possible to obtain quantitative insight into the relative energetics of different pore sizes due to the high mobility of the ions inside the pores, it is possible to determine the energy difference associated with the average in-pore and ex-pore environments assuming [population occupancy](#) of the two states according to the Boltzmann distribution using

$$C_{in}/C_{ex} = e^{-\frac{\Delta G_{in-ex}}{k_B T}} \quad (24)$$

where  $\Delta G_{in-ex}$  is the average free energy difference between the in-pore and ex-pore environments,  $k_B$  is the Boltzmann constant and  $T$  is the temperature. Using this simplified model,  $\Delta G_{in-ex}$  at 298 K for 1M NaCl is found to be 5.1 kJ mol<sup>-1</sup> for PDC with 21% burn-off, reducing to 2.2 kJ mol<sup>-1</sup> for 55% burn-off. On the basis of MD simulations, Beckstein *et al.* have calculated significantly higher values of  $\Delta G = 9 - 18$  kJ mol<sup>-1</sup> for the entry of hydrated Na<sup>+</sup> ions to micropores between 1.1 – 2.0 nm in width.[14] However, we note that the MD simulations were effectively carried out at infinite dilution, while  $\Delta G_{in-ex}$  determined from the NMR measurements takes into account the chemical potentials of both in-pore and ex-pore environments. The non-zero concentration of the ex-pore electrolyte in the

experimental system should significantly lower the energy difference between the in-pore and ex-pore environments. In addition, we note that the chemical potential of aqueous NaCl solution reduces by more than  $10 \text{ kJ mol}^{-1}$  in the range  $1 - 0.1 \text{ M}$ .<sup>[75, 76]</sup> Since the predicted  $\Delta G$  values for entry of hydrated  $\text{Na}^+$  to micropores are of comparable magnitude, it is highly feasible that changing the concentration over this range will lead to significant emptying of the smaller micropores in favour of lower energy adsorption sites in the larger micropores and mesopores.

The redistribution of ions within the porous network also explains the significant 1.65 ppm change in the  $^{23}\text{Na}$  NICS observed for the 0.1 M electrolyte upon saturation of the sample (Figure 129). Before saturation, the average in-pore concentration is forced to equal that of the neat electrolyte, and this will dictate the distribution of ions between large and small pores. However, after saturation, the system becomes free to redistribute ions between the ex-pore and in-pore environments as well as within the porous network. Since the in-pore environment is energetically less favourable than the ex-pore environment, ions are expected to move from the in-pore to the ex-pore environment until the point where the energetic penalty of the increased ex-pore chemical potential balances the energetic gain from the redistribution of in-pore ions to favour occupancy of the mesopores. Based on the hypothesis that the redistribution of ions is driven by the higher adsorption energy in small pores, PDCs with a higher proportion of small pores should be expected to produce a more pronounced redistribution upon saturation and therefore larger NICS reduction. To test this experimentally, the same saturation experiments were conducted in a sample with a smaller burn-off of 36%, and hence a higher proportion of small pores relative to big pores (see Supporting Information). Upon saturation, the integral of the in-pore cation resonance decreases and the NICS is reduced by a larger value of 2.17 ppm, which is consistent with more ions being moved towards bigger pores and out of the pore network. We note that the NICS for the  $\text{H}_2\text{O}$  solvent molecules again remained unchanged upon saturation.

## Discussion

One important consequence of the specific ion and concentration effects observed in this work is the potential influence on the charging mechanism in electrochemical double layer devices. Despite traditionally being assumed to function through ion adsorption, recent studies have shown that charge can be stored in microporous electrodes through at least three different mechanisms: counter-ion adsorption, ion exchange, and co-ion expulsion.[8, 27, 77, 78] The precise mechanism for a particular system is expected to be strongly influenced by the occupancy of the micropores in the absence of an applied potential. For pores that contain ions prior to charging, either of the three mechanisms is possible in principle, whereas pores that are initially empty can only charge through adsorption of counter-ions from the ex-pore electrolyte. Therefore, for large and strongly hydrated ions such as  $\text{Na}^+$  which have a suppressed in-pore concentration prior to charging, counter-ion adsorption may be favoured over other charging mechanisms. Kondrat [and Kornyshev \*et al.\*](#) have shown using mean-field theory that the existence of a superionic state during counter-ion adsorption in co-ion deficient nanopores can increase the differential capacitance up to the point where the pores reach saturation.[79] This may help explain why Li- and Na-based aqueous electrolytes (which have a suppressed in-pore cation concentration at zero potential) show superior capacitance in aqueous supercapacitor devices.[2] Furthermore, mean-field theory calculations [and Monte Carlo have also shown that energy storage and charging dynamics can be increased if ions are thermodynamically disfavoured from entering the pores in the absence of an applied potential](#)~~also predicted significant increases in charging dynamics for “ionophobic” pores that are initially unfilled by ions prior to charging.~~[15, 16, 80] [Indeed, it has been shown that the use of so-called ionophobic pores \(which are initially unfilled with ions prior to charging\) can store energy more efficiently at high electrode polarisations and charge significantly faster.](#) It may therefore be possible to tailor the charging dynamics of supercapacitors by carefully controlling both the relative pore / ion size and concentration to maximise the suppression of the in-pore ion population ~~prior to charging~~[in the](#)

[absence of an applied potential](#), whilst still allowing electrosorption to occur [when charging commences](#).

In addition to affecting the charge storage properties of supercapacitors, the zero-potential in-pore ion population may have important implications for the desalination efficiency of CDI devices. For  $\text{Li}^+$  and  $\text{Na}^+$ , the favoured counter-ion adsorption mechanism should be beneficial since the aim in CDI is to remove ions from the electrolyte solution. However, for  $\text{Cs}^+$ , which is one of the main contaminants in nuclear waste effluents, the increased propensity for micropore filling prior to charging may favour ion exchange or co-ion expulsion. In principle, these charging mechanisms should result in no decrease or even an increase in the concentration of the bulk electrolyte since co-ions are ejected from the micropores during charging. Therefore in order to employ CDI for the treatment of water contaminated with nuclear waste may require careful design and optimisation of the micropore structure to minimise entry of the ions prior to charging.

## Conclusions

In this work we have performed a systematic study of aqueous electrolytes adsorbed on PDCs [in the absence of an applied potential](#). Our experiments have provided fundamental insight into the factors affecting the NICS in these systems and highlight important effects that must be taken into account when studying these systems by NMR spectroscopy. We have found that careful control of the carbonisation and activation procedure is necessary to obtain homogenous PDC samples with evenly activated particles. For homogeneously activated PDCs the magnitude of the NICS for a particular species [for  \$\text{H}\_2\text{O}\$  and  \$\text{Li}^+\$  and  \$\text{Na}^+\$](#)  follows the expected pore size dependence; ~~;~~ however, comparison [of NICS between](#) different cationic and solvent species, is less straightforward because the magnitude of the apparent NICS is [also](#) affected by differences in relative ion size and desolvation. We have also found that the NICS [of](#) cationic species shows a dependence on the

electrolyte concentration. This can be rationalised in terms of the thermodynamic redistribution of ions between pores of different sizes arising from the pore-size dependent energy barrier for pore entry [in the absence of an applied potential, and links to the recently developed concept of pore ionophobicity. Our results indicate that the PDC micropores are effectively ionophobic with respect to hydrated Li<sup>+</sup> and Na<sup>+</sup> ions, leading to expulsion from the smallest micropores at low electrolyte concentrations.](#)

–Overall this work highlights that a variety of factors can influence the apparent NICS of in-pore species and these effects must be carefully accounted for when using it to gain information about the carbon structure or ion behaviour. Furthermore, the information provided by NICS measurements has potentially important implications for understanding ion behaviour and charging mechanisms in electrochemical devices.

## References

- [1] P. Simon and Y. Gogotsi, *Acc. Chem. Res.* 46 (2013), 1094-1103.
- [2] K. Fic, G. Lota, M. Meller and E. Frackowiak, *Energy Environ. Sci.* 5 (2012), 5842-5850.
- [3] Q. Gao, L. Demarconnay, E. Raymundo-Piñero and F. Béguin, *Energy Environ. Sci.* 5 (2012), 9611-9617.
- [4] S. Vaquero, J. Palma, M. Anderson and R. Marcilla, *International Journal of Electrochemical Science* 8 (2013), 10293-10307.
- [5] Z. Chang, Y.Q. Yang, M.X. Li, X.W. Wang and Y.P. Wu, *Journal of Materials Chemistry A* 2 (2014), 10739-10755.
- [6] B. Dyatkin, V. Presser, M. Heon, M.R. Lukatskaya, M. Beidaghi and Y. Gogotsi, *Chemsuschem* 6 (2013), 2269-2280.
- [7] S. Porada, L. Borchardt, M. Oschatz, M. Bryjak, J.S. Atchison, K.J. Keesman, S. Kaskel, P.M. Biesheuvel and V. Presser, *Energy Environ. Sci.* 6 (2013), 3700-3712.
- [8] M.E. Suss, S. Porada, X. Sun, P.M. Biesheuvel, J. Yoon and V. Presser, *Energy Environ. Sci.* 8 (2015), 2296-2319.
- [9] C.D. Williams and P. Carbone, *Environmental Science & Technology* 50 (2016), 3875-3881.
- [10] L.A. Richards, A.I. Schäfer, B.S. Richards and B. Corry, *Phys. Chem. Chem. Phys.* 14 (2012), 11633-11638.
- [11] H. Liu, C.J. Jameson and S. Murad, *Molecular Simulation* 34 (2008), 169-175.
- [12] C. Song and B. Corry, *J. Phys. Chem. B* 113 (2009), 7642-7649.
- [13] L.A. Richards, A.I. Schafer, B.S. Richards and B. Corry, *Small* 8 (2012), 1701-1709.
- [14] O. Beckstein, K. Tai and M.S.P. Sansom, *J. Am. Chem. Soc.* 126 (2004), 14694-14695.
- [15] S. Kondrat, P. Wu, R. Qiao and A.A. Kornyshev, *Nature Materials* 13 (2014), 387-393.
- [16] S. Kondrat and A.A. Kornyshev, *Nanoscale Horizons* 1 (2016), 45-52.
- [17] M.D. Levi, G. Salitra, N. Levy, D. Aurbach and J. Maier, *Nature Materials* 8 (2009), 872-875.
- [18] S. Sigalov, M.D. Levi, G. Salitra, D. Aurbach, A. Janes, E. Lust and I.C. Halalay, *Carbon* 50 (2012), 3957-3960.
- [19] M.D. Levi, N. Levy, S. Sigalov, G. Salitra, D. Aurbach and J. Maier, *J. Am. Chem. Soc.* 132 (2010), 13220-13222.
- [20] W.-Y. Tsai, P.-L. Taberna and P. Simon, *J. Am. Chem. Soc.* 136 (2014), 8722-8728.
- [21] M.D. Levi, S. Sigalov, D. Aurbach and L. Daikhin, *J. Phys. Chem. C* 117 (2013), 14876-14889.
- [22] N. Shpigel, M.D. Levi, S. Sigalov, D. Aurbach, L. Daikhin and V. Presser, *Journal of Physics-Condensed Matter* 28 (2016).
- [23] M.D. Levi, N. Shpigel, S. Sigalov, V. Dargel, L. Daikhin and D. Aurbach, *Electrochim. Acta* 232 (2017), 271-284.
- [24] N. Shpigel, M.D. Levi, S. Sigalov, L. Daikhin and D. Aurbach, *Acc. Chem. Res.* 51 (2018), 69-79.
- [25] S. Boukhalifa, D. Gordon, L.L. He, Y.B. Melnichenko, N. Nitta, A. Magasinski and G. Yushin, *Acs Nano* 8 (2014), 2495-2503.
- [26] S. Boukhalifa, L. He, Y.B. Melnichenko and G. Yushin, *Angew. Chem. Int. Ed.* 52 (2013), 4618-4622.
- [27] J.M. Griffin, A.C. Forse, H. Wang, N.M. Trease, P.L. Taberna, P. Simon and C.P. Grey, *Faraday Discuss.* 176 (2014), 49-68.
- [28] J.M. Griffin, A.C. Forse and C.P. Grey, *Solid State Nucl. Magn. Reson.* 74-75 (2016), 16-35.

- [29] R.K. Harris, T.V. Thompson, P.R. Norman and C. Pottage, *Journal of the Chemical Society-Faraday Transactions* 92 (1996), 2615-2618.
- [30] R.K. Harris, T.V. Thompson, P.R. Norman and C. Pottage, *Carbon* 37 (1999), 1425-1430.
- [31] L. Borchardt, M. Oschatz, S. Paasch, S. Kaskel and E. Brunner, *Phys. Chem. Chem. Phys.* 15 (2013), 15177-15184.
- [32] A.C. Forse, J.M. Griffin, H. Wang, N.M. Trease, V. Presser, Y. Gogotsi, P. Simon and C.P. Grey, *Phys. Chem. Chem. Phys.* 15 (2013), 7722-7730.
- [33] M. Deschamps, E. Gilbert, P. Azais, E. Raymundo-Pinero, M.R. Ammar, P. Simon, D. Massiot and F. Beguin, *Nature Materials* 12 (2013), 351-358.
- [34] R.J. Anderson, T.P. McNicholas, A. Kleinhammes, A.M. Wang, J. Liu and Y. Wu, *J. Am. Chem. Soc.* 132 (2010), 8618-8626.
- [35] Y.Z. Xing, Z.X. Luo, A. Kleinhammes and Y. Wu, *Carbon* 77 (2014), 1132-1139.
- [36] A.C. Forse, J.M. Griffin, V. Presser, Y. Gogotsi and C.P. Grey, *J. Phys. Chem. C* 118 (2014), 7508-7514.
- [37] A.C. Forse, C. Merlet, P.K. Allan, E.K. Humphreys, J.M. Griffin, M. Aslan, M. Zeiger, V. Presser, Y. Gogotsi and C.P. Grey, *Chem. Mater.* 27 (2015), 6848-6857.
- [38] C. Merlet, A.C. Forse, J.M. Griffin, D. Frenkel and C.P. Grey, *J. Chem. Phys.* 142 (2015).
- [39] N. Fulik, F. Hippauf, D. Leistenschneider, S. Paasch, S. Kaskel, E. Brunner and L. Borchardt, *Energy Storage Materials* 12 (2018), 183-190.
- [40] I.P.P. Cansado, F. Goncalves, J.M.V. Nabais, M. Carrott and P.J.M. Carrott, *Fuel Process. Technol.* 90 (2009), 232-236.
- [41] I.P.P. Cansado, F. Goncalves, P.J.M. Carrott and M. Carrott, *Carbon* 45 (2007), 2454-2455.
- [42] T.P. McNicholas, A.M. Wang, K. O'Neill, R.J. Anderson, N.P. Stadie, A. Kleinhammes, P. Parilla, L. Simpson, C.C. Ahn, Y.Q. Wang, Y. Wu and J. Liu, *J. Phys. Chem. C* 114 (2010), 13902-13908.
- [43] H.J. Wang, A. Kleinhammes, T.P. McNicholas, J. Liu and Y. Wu, *J. Phys. Chem. C* 118 (2014), 8474-8480.
- [44] Z.X. Luo, Y.Z. Xing, Y.C. Ling, A. Kleinhammes and Y. Wu, *Nature Communications* 6 (2015).
- [45] Z.X. Luo, Y.Z. Xing, S.B. Liu, Y.C. Ling, A. Kleinhammes and Y. Wu, *J. Phys. Chem. Lett.* 6 (2015), 5022-5026.
- [46] Y. Song, Y. Chong, A. Raghavan, Y. Xing, Y. Ling, A. Kleinhammes and Y. Wu, *J. Phys. Chem. C* 121 (2017), 8504-8509.
- [47] F. Rodríguez-Reinoso and M. Molina-Sabio, *Carbon* 30 (1992), 1111-1118.
- [48] C.-F. Chang, C.-Y. Chang and W.-T. Tsai, *J. Colloid Interface Sci.* 232 (2000), 45-49.
- [49] D.G. Cory and W.M. Ritchey, *J. Magn. Reson.* 80 (1988), 128-132.
- [50] D. Marion, M. Ikura, R. Tschudin and A. Bax, *J. Magn. Reson.* 85 (1989), 393-399.
- [51] D. Massiot, F. Fayon, M. Capron, I. King, S. Le Calvé, B. Alonso, J.-O. Durand, B. Bujoli, Z. Gan and G. Hoatson, *Magn. Reson. Chem.* 40 (2002), 70-76.
- [52] M. Findeisen, T. Brand and S. Berger, *Magn. Reson. Chem.* 45 (2007), 175-178.
- [53] R.M. Cotts, M.J.R. Hoch, T. Sun and J.T. Markert, *J. Magn. Reson.* 83 (1989), 252-266.
- [54] M.A. Connell, A.L. Davis, A.M. Kenwright and G.A. Morris, *Analytical and Bioanalytical Chemistry* 378 (2004), 1568-1573.
- [55] J. VandeVondele, M. Krack, F. Mohamed, M. Parrinello, T. Chassaing and J. Hutter, *Comput. Phys. Commun.* 167 (2005), 103-128.
- [56] J. Hutter, M. Iannuzzi, F. Schiffmann and J. VandeVondele, *Wiley Interdisciplinary Reviews-Computational Molecular Science* 4 (2014), 15-25.
- [57] S. Nosé, *Mol. Phys.* 52 (1984), 255-268.
- [58] G. Lippert, J. Hutter and M. Parrinello, *Theor. Chem. Acc.* 103 (1999), 124-140.
- [59] J.P. Perdew, K. Burke and M. Ernzerhof, *Phys. Rev. Lett.* 77 (1996), 3865-3868.
- [60] S. Grimme, J. Antony, S. Ehrlich and H. Krieg, *J. Chem. Phys.* 132 (2010).
- [61] J. VandeVondele and J. Hutter, *J. Chem. Phys.* 127 (2007).

- [62] J.A. Morrone and R. Car, *Phys. Rev. Lett.* 101 (2008).
- [63] D. Di Tommaso and N.H. de Leeuw, *Cryst. Growth. Des.* 10 (2010), 4292-4302.
- [64] R. Atta-Fynn, D.F. Johnson, E.J. Bylaska, E.S. Ilton, G.K. Schenter and W.A. de Jong, *Inorg. Chem.* 51 (2012), 3016-3024.
- [65] S. Bogatko, E. Cauet, E. Bylaska, G. Schenter, J. Fulton and J. Weare, *Chemistry-a European Journal* 19 (2013), 3047-3060.
- [66] P. Nichols, E.J. Bylaska, G.K. Schenter and W. de Jong, *J. Chem. Phys.* 128 (2008).
- [67] M.J. McGrath, I.F.W. Kuo and J.I. Siepmann, *Phys. Chem. Chem. Phys.* 13 (2011), 19943-19950.
- [68] I. Bako, J. Hutter and G. Palinkas, *J. Chem. Phys.* 117 (2002), 9838-9843.
- [69] A.C. Forse, J.M. Griffin, C. Merlet, J. Carretero-Gonzalez, A.R.O. Raji, N.M. Trease and C.P. Grey, *Nature Energy* 2 (2017).
- [70] J.D. Halliday, R.E. Richards and R.R. Sharp, *Proceedings of the Royal Society of London. Series A, Mathematical and Physical Sciences* 313 (1969), 45-69.
- [71] W.J. DeWitte, L. Liu, E. Mei, J.L. Dye and A.I. Popov, *J. Solution Chem.* 6 (1977), 337-348.
- [72] A. Abragam and R.V. Pound, *Physical Review* 92 (1953), 943-962.
- [73] M. Gerken, J.A. Boatz, A. Kornath, R. Haiges, S. Schneider, T. Schroer and K.O. Christe, *J. Fluorine Chem.* 116 (2002), 49-58.
- [74] L.A. Richards, B.S. Richards, B. Corry and A.I. Schäfer, *Environmental Science & Technology* 47 (2013), 1968-1976.
- [75] F. Moučka, I. Nezbeda and W.R. Smith, *Journal of Chemical Theory and Computation* 11 (2015), 1756-1764.
- [76] W.J. Hamer and Y.C. Wu, *J. Phys. Chem. Ref. Data* 1 (1972), 1047-1100.
- [77] J.M. Griffin, A.C. Forse, W.Y. Tsai, P.L. Taberna, P. Simon and C.P. Grey, *Nature Materials* 14 (2015), 812-+.
- [78] A.C. Forse, C. Merlet, J.M. Griffin and C.P. Grey, *J. Am. Chem. Soc.* 138 (2016), 5731-5744.
- [79] S. Kondrat and A. Kornyshev, *Journal of Physics-Condensed Matter* 23 (2011).
- [80] S. Kondrat and A. Kornyshev, *J. Phys. Chem. C* 117 (2013), 12399-12406.

|

